Model reduction for flight dynamics simulations using computational fluid dynamics

Giampaolo Pagliuca[a,*], Sebastian Timme[a]

[a] *University of Liverpool, Liverpool L69 3GH, United Kingdom*

Abstract

Multidisciplinary simulation involving flight dynamics and computational fluid dynamics is required for high-fidelity gust loads analysis in transonic flow. However, the main limitation to a more routine use is prohibitive computational cost involved. A promising trade-off between accuracy and low-cost is model reduction of high-fidelity methods. Thus investigation of such reduction of coupled models is presented. The reduction technique relies on an expansion of the full order non-linear residual function in a truncated Taylor series and subsequent projection onto a small modal basis. Two procedures are discussed to obtain modes for the projection. First, an operator-based identification is exploited to calculate eigenpairs of the coupled Jacobian matrix related to the flight dynamics degrees-of-freedom. Secondly, proper orthogonal decomposition is used as a data-based method to obtain modes representing the system subject to external disturbance such as gusts. Benefits and limitations of the various methods are investigated by analysing results for initial disturbance and gust encounter simulations. Overall, reduced order models based on the presented approaches are able to retain the accuracy of the high-fidelity tools to predict accurately flight dynamics responses and loads while reducing the computational cost up to two orders of magnitude.

Keywords: Reduced order model, Flight dynamics, Computational fluid dynamics, Modal identification, Gust encounter simulations

1. Introduction

Aircraft design and certification requires an accurate prediction of gust loads for many points covering the flight envelope [1]. Multidisciplinary analyses involving, among others, flight dynamics (FD), flexible structures and aerodynamics are needed [2]. Nowadays, these simulations adopt linear potential methods as aerodynamic model and offer low fidelity at affordable computational cost. Such coupling of flight dynamics, flexible structures and unsteady aerodynamics for gust response analysis was achieved, for instance, in [3]

*Corresponding author

Email address: g.pagliuca@liverpool.ac.uk (Giampaolo Pagliuca)

using unsteady lifting line theory in the subsonic regime. Various approaches for coupled simulations were proposed for gust analysis of HALE (High Altitude, Long Endurance) configurations [4, 5] since flight dynamics effects are essential to predict accurately those systems' behaviour. Free-flight effects can also be included directly in the linear aerodynamics equations with correction terms accounting for body acceleration, as suggested in [6, 7]. However, the work described so far exclusively relies on low fidelity aerodynamic models to perform multidisciplinary simulations.

Application in the transonic regime requires high-fidelity aerodynamics based on computational fluid dynamics (CFD), which can describe non-linear flow phenomena like shock waves, with a higher computational cost to be paid. An example of simulations for a manoeuvring aircraft in transonic flow is presented in [8], running a CFD solver alongside a structural modal solver in a closed loop. The manoeuvre was pre-defined so that time-varying flight dynamics parameters such as angle-of-attack are imposed onto the CFD solver at each time-step. A similar approach based on two distinct and interacting subsystems was also applied in [9] to cope with large static displacements in transonic flow. Although these studies provide an effective way to cope with pre-defined manoeuvres or static problems, an extension to unsteady gust simulations is needed. For such simulations, flight dynamics unknowns must be calculated at each time-step using the most recent values of aerodynamic forces which, in turn, depend also on the gust disturbance. Moreover, aerodynamics also depends on flight dynamics unknowns, leading to a two-way coupled problem. It was shown that flight dynamics effects cannot be neglected in high-fidelity gust loads analysis [10]. In addition, comparison between CFD and tools currently used in industrial practice highlighted the limitations of the latter. With feasibility for an industry-scale adoption of multidisciplinary analyses based on CFD already demonstrated, the main obstacle remains computational cost. A first reduction of computational cost required for CFD has already been obtained using linearised frequency domain (LFD) formulations for both aerodynamic response only [11] and fluid-structure coupled simulations [12, 13]. However, more rapid methods that allow for high-fidelity accuracy in transonic flow are still desirable.

Model reduction of high-fidelity methods is a good alternative to balance cost and accuracy. Owing to the fact that the flight dynamics equations are of low dimension, high-fidelity aerodynamics is typically represented as dynamic derivatives [14], possibly calculated using the LFD approach. The flight dynamics response is then obtained by integrating the equations of motion in time using rigid-body modes and an interpolation of the dynamic derivatives at each time-step. Other techniques are possible and a summary of reduction methods in the flight dynamics context is provided in [15]. These techniques usually are applied to the aerodynamics equations only. Another possible approach operates on the coupled system as a whole. It manipulates the full order, coupled non-linear residual function expanded in a Taylor series with a projection on an appropriate modal basis resulting in a monolithic reduced model [16]. The projection method produces a versatile reduced order model which facilitates a comprehensive study of the coupled system. Previous application includes the simulation of coupled structural and aerodynamic systems using linear potential aerodynamics for gust encounter analysis and robust control [16, 17]. An extension to CFD is possible by calculating modes for the projection using the Schur complement method [18],

and this was applied to a flexible aircraft for aeroelastic analyses in transonic flow in [13]. This formulation can also be used for structural non-linearities [19] and might be expanded to account for aerodynamic non-linearities leading to limit cycle oscillations [20].

In this paper, the model reduction technique based on modal projection is introduced for the flight dynamics problem with application to free-flight test cases in the transonic regime. Two procedures to calculate modes for the projection are investigated. First, flight dynamics modes, also known as dynamic stability modes [21, 22], are identified with an operator-based method. Exact values of frequency and damping for the flight dynamics modes are unknown a priori since they depend on flow parameters and structural properties. These modes correspond to a few eigenpairs of the coupled Jacobian matrix. Calculating the complete eigenspectrum of the coupled system and applying a trial-and-error approach to find the flight dynamics eigenpairs is prohibitive even for small-sized test cases. An operator-based identification procedure is proposed instead to compute these specific eigenpairs directly. Secondly, modes for the projection are calculated with a frequency domain formulation of proper orthogonal decomposition (POD) [23]. POD was previously applied to an aerodynamics-only system for gust encounter simulations of a large civil aircraft in transonic flow [24]. Here, POD is used for the flight dynamics problem subject to external disturbances in order to obtain both flight dynamic and aerodynamic responses. It is referred to as data-based identification since the system is probed at various frequencies.

The paper proceeds in Section 2 with a description of the numerical formulation. The reduction method is derived and the two identification procedures are presented. Non-linear, time-domain simulations coupling CFD aerodynamics with flight dynamics equations of motion are adopted to provide reference solutions, whereas constructing the reduced models is accelerated by using LFD methods throughout in the paper. In Section 3 results are presented for two two-dimensional test cases. The identification of flight dynamics modes is described in detail for a NACA 0012 aerofoil in transonic flow solving the Euler equations. The size of this test case allows for an in-depth analysis of problems which can arise during the identification. Model reduction for longitudinal dynamics in transonic flow modelled with Reynolds-averaged Navier–Stokes (RANS) equations is subsequently exploited and applied to gust encounter analysis of a tandem aerofoil configuration representing the dynamics of a large civil aircraft.

2. Numerical approach

2.1. Full order model and model reduction

Rigid-body dynamics is described by the equations of motion obtained directly from Newton's second law [21]. Denoting $\boldsymbol{w}_r$ as the vector containing n_r flight dynamics unknowns and $\boldsymbol{R}_r$ as the corresponding non-linear residual function, the flight dynamics equations are formulated as a first order ordinary differential equation in time t,

$$\frac{\mathrm{d}\boldsymbol{w}_r}{\mathrm{d}t} = \boldsymbol{R}_r(\boldsymbol{w}_f, \boldsymbol{w}_r) \tag{1}$$

with the vector $\boldsymbol{w}_f$ containing the n_f fluid unknowns. Specifically, the residual vector $\boldsymbol{R}_r$ is written as

$$\boldsymbol{R}_r(\boldsymbol{w}_f, \boldsymbol{w}_r) = \boldsymbol{f}_e(\boldsymbol{w}_r) + C\boldsymbol{f}_a(\boldsymbol{w}_f, \boldsymbol{w}_r) \tag{2}$$

with $\boldsymbol{f}_a$ representing aerodynamic forces. The formulation of the vector function $\boldsymbol{f}_e$ depends on the reference frame (absolute or relative formulation) since it might include Coriolis effects [22] besides additional external forces such as gravity. The matrix C accounts for the coupling between the degrees-of-freedom and it contains information about geometric properties of the system. The non-linear equations describing aerodynamics are similarly written in a semi-discrete form as

$$\frac{\mathtt{d}\boldsymbol{w}_f}{\mathtt{d}t} = \boldsymbol{R}_f(\boldsymbol{w}_f, \boldsymbol{w}_r, \boldsymbol{u}_d) \tag{3}$$

where $\boldsymbol{R}_f$ is the non-linear residual corresponding to the fluid unknowns and $\boldsymbol{u}_d$ represents a possible external disturbance such as gusts. Denoting $\boldsymbol{w} = [\boldsymbol{w}_f^T, \boldsymbol{w}_r^T]^T$ as the vector of unknowns of the coupled system, the state-space equations of dimension $n = n_f + n_r$ can be combined as

$$\frac{\mathtt{d}\boldsymbol{w}}{\mathtt{d}t} = \boldsymbol{R}\left(\boldsymbol{w}, \boldsymbol{u}_d\right) \tag{4}$$

where $\boldsymbol{R}$ is the corresponding coupled non-linear residual vector. Reference solutions are obtained throughout the paper by integrating the full order model (FOM) defined in Eq. (4).

The system in Eq. (4) is expanded in a first order Taylor series around an equilibrium state with $\boldsymbol{R}(\boldsymbol{w}_0, \boldsymbol{u}_{d0}) = 0$,

$$\boldsymbol{R}(\boldsymbol{w}, \boldsymbol{u}_d) = A\,\widetilde{\boldsymbol{w}} + \frac{\partial \boldsymbol{R}}{\partial \boldsymbol{u}_d}\widetilde{\boldsymbol{u}}_d + O\left(|\widetilde{\boldsymbol{w}}|^2, |\widetilde{\boldsymbol{u}}_d|^2\right) \tag{5}$$

where $\boldsymbol{w}(t) = \boldsymbol{w}_0 + \widetilde{\boldsymbol{w}}(t)$ and accordingly $\boldsymbol{u}_d(t) = \boldsymbol{u}_{d0} + \widetilde{\boldsymbol{u}}_d(t)$. The Jacobian matrix A of dimension $n \times n$ is partitioned into blocks

$$A = \begin{pmatrix} A_{ff} & A_{fr} \\ A_{rf} & A_{rr} \end{pmatrix} \tag{6}$$

with

$$A_{ff} = \frac{\partial \boldsymbol{R}_f}{\partial \boldsymbol{w}_f} \qquad A_{fr} = \frac{\partial \boldsymbol{R}_f}{\partial \boldsymbol{w}_r} \qquad A_{rf} = C\frac{\partial \boldsymbol{f}_a}{\partial \boldsymbol{w}_f} \qquad A_{rr} = \frac{\partial \boldsymbol{f}_e}{\partial \boldsymbol{w}_r} + C\frac{\partial \boldsymbol{f}_a}{\partial \boldsymbol{o}}\frac{\partial \boldsymbol{o}}{\partial \boldsymbol{w}_r} \tag{7}$$

The diagonal blocks A_{ff} and A_{rr} are fluid and flight dynamics Jacobian matrices, respectively, whereas the off-diagonal blocks describe the coupling terms. Specifically, the matrix A_{rf} describes the dependence of the aerodynamic forces on the fluid unknowns and A_{fr} represents fluid excitation due to the flight dynamics degrees-of-freedom. The term $\frac{\partial \boldsymbol{f}_a}{\partial \boldsymbol{o}}$ relates a change of aerodynamic forces to a rotation of surface normals $\boldsymbol{o}$ while keeping the flow variables fixed. The term $C\frac{\partial \boldsymbol{f}_a}{\partial \boldsymbol{o}}\frac{\partial \boldsymbol{o}}{\partial \boldsymbol{w}_r}$ is neglected in the current investigation since it is small in comparison to $\frac{\partial \boldsymbol{f}_e}{\partial \boldsymbol{w}_r}$ which contains structural mass and moment of inertia [12].

Two variants of the LFD approach are extensively used in the paper. The first for coupled problems is obtained by substituting Eq. (5) into Eq. (4) and translating to frequency domain with $\widetilde{\boldsymbol{w}}(t) = \hat{\boldsymbol{w}} e^{i\omega t}$ and $\widetilde{\boldsymbol{u}}_d = \hat{\boldsymbol{u}}_d e^{i\omega t}$,

$$(A - i\omega I)\,\hat{\boldsymbol{w}} = -\frac{\partial \boldsymbol{R}}{\partial \boldsymbol{u}_d}\,\hat{\boldsymbol{u}}_d \tag{8}$$

This allows the calculation of both aerodynamic and flight dynamic responses to harmonic external disturbances at frequency ω since the coupled Jacobian matrix is involved. The second formulation for the aerodynamics only is derived considering the homogeneous form of Eq. (8) with $\widetilde{\boldsymbol{u}}_d = 0$. The partitioning in Eq. (6) is applied, resulting in $\widetilde{\boldsymbol{w}}_f(t) = \hat{\boldsymbol{w}}_f e^{i\omega t}$ and $\widetilde{\boldsymbol{w}}_r(t) = \hat{\boldsymbol{w}}_r e^{i\omega t}$. Isolating the fluid dynamics unknowns leads to

$$(A_{ff} - i\omega I)\,\hat{\boldsymbol{w}}_f = -A_{fr}\hat{\boldsymbol{w}}_r \tag{9}$$

This equation is particularly useful to compute the aerodynamic responses to harmonic excitation in the flight dynamics degrees-of-freedom and this is the case when calculating the dynamic derivatives. It can be expanded to any harmonic motion with damping γ and frequency ω by assuming $\widetilde{\boldsymbol{w}}_f(t) = \hat{\boldsymbol{w}}_f e^{(\gamma+i\omega)t}$ and $\widetilde{\boldsymbol{w}}_r(t) = \hat{\boldsymbol{w}}_r e^{(\gamma+i\omega)t}$.

The model reduction is performed by projecting the Taylor series in Eq. (5) on a smaller modal basis [16]. The bases Φ and Ψ are built by choosing m appropriate modes,

$$\text{right: } \Phi = \begin{pmatrix} \boldsymbol{\phi}^{(1)}, & \boldsymbol{\phi}^{(2)}, & \dots, & \boldsymbol{\phi}^{(m)} \end{pmatrix} \quad \text{left: } \Psi = \begin{pmatrix} \boldsymbol{\psi}^{(1)}, & \boldsymbol{\psi}^{(2)}, & \dots, & \boldsymbol{\psi}^{(m)} \end{pmatrix} \tag{10}$$

scaled to satisfy the conditions

$$\langle \boldsymbol{\phi}^{(j)}, \boldsymbol{\phi}^{(j)} \rangle = 1 \qquad \text{and} \qquad \langle \boldsymbol{\psi}^{(j)}, \boldsymbol{\phi}^{(j)} \rangle = 1 \qquad\qquad \forall j \in [1, m] \tag{11}$$

where the Hermitian inner product $\langle \boldsymbol{x}, \boldsymbol{y} \rangle$ is defined as $\boldsymbol{x}^H \boldsymbol{y}$. The projection is performed with the transformation

$$\widetilde{\boldsymbol{w}} = \Phi \boldsymbol{z}, \quad \boldsymbol{z} \in \mathbb{C}^m \tag{12}$$

and pre-multiplying with the left modal basis Ψ. Including complex conjugate pairs in the modal basis in Eq. (10) gives a real-valued vector $\widetilde{\boldsymbol{w}}$ in Eq. (12). This simplifies reconstructing physical quantities from the reduced model while doubling its negligible computational cost. The reduced order model (ROM) is then expressed as

$$\Psi^H \Phi \frac{\mathrm{d}\boldsymbol{z}}{\mathrm{d}t} = \Psi^H A \Phi\, \boldsymbol{z} + \Psi^H \frac{\partial \boldsymbol{R}}{\partial \boldsymbol{u}_d}\,\widetilde{\boldsymbol{u}}_d \tag{13}$$

and integrated in time to obtain time-domain response $z(t)$. Assuming harmonic excitation $\widetilde{\boldsymbol{u}}_d = \hat{\boldsymbol{u}}_d e^{i\omega t}$ and harmonic response $\boldsymbol{z}(t) = \hat{\boldsymbol{z}} e^{i\omega t}$, Eq. (13) can also be rewritten in frequency domain,

$$\Psi^H (A - i\omega I)\,\Phi \hat{\boldsymbol{z}} = -\Psi^H \frac{\partial \boldsymbol{R}}{\partial \boldsymbol{u}_d}\,\hat{\boldsymbol{u}}_d \tag{14}$$

Exploiting Eq. (14) is more convenient for responses to sinusoidal external disturbances and it is used for the data-based approaches. Equation (13) is adopted for the operator-based ROM with Eq. (14) leading to the same results.

The modal bases in Eq. (10) must be built from modes representing the dominating system behaviour. Two procedures, named operator-based and data-based modal identification, are proposed in the following to calculate these modes.

2.2. Operator-based modal identification

The system in Eq. (4) is expanded by means of Eq. (5) and translated into Laplace domain with complex-valued variable λ. The external disturbance $\boldsymbol{u}_d$ is zero for operator-based identification. This leads to the direct and adjoint eigenvalue problems,

$$\left(A - \lambda^{(j)} I\right) \boldsymbol{\phi}^{(j)} = 0 \qquad \text{and} \qquad \left(A^T - \lambda^{(j)} I\right) \bar{\boldsymbol{\psi}}^{(j)} = 0 \qquad \forall j \in [1, m] \tag{15}$$

where $(\lambda^{(j)}, \boldsymbol{\phi}^{(j)})$ and $(\lambda^{(j)}, \boldsymbol{\psi}^{(j)})$ are the corresponding eigenpairs. A subset of m direct and adjoint eigenvectors related to flight dynamics degrees-of-freedom is included in the modal bases for the model reduction. Notice that in this case the conditions in Eq. (11) are satisfied due to the bi-orthogonality of eigenvectors,

$$\langle \boldsymbol{\psi}^{(j)}, \boldsymbol{\phi}^{(k)} \rangle = \delta_{jk} \qquad \text{and} \qquad \langle \boldsymbol{\psi}^{(j)}, \bar{\boldsymbol{\phi}}^{(k)} \rangle = 0 \qquad \forall j, k \in [1, m] \tag{16}$$

where δ_{jk} is the Kronecker delta. The small eigenvalue problem of dimension n_r resulting from the flight dynamics part of the direct eigenproblem in Eq. (15) is

$$\left[\left(A_{rr} - \lambda^{(j)} I\right) - \beta A_{rf} \left(A_{ff} - \lambda^{(j)} I\right)^{-1} A_{fr} \right] \boldsymbol{\phi}_r^{(j)} = S(\lambda^{(j)}) \boldsymbol{\phi}_r^{(j)} = 0 \tag{17}$$

where $S(\lambda^{(j)})$ is the spectral Schur complement of A with respect to flight dynamics degrees-of-freedom. An artificial weighting factor β is introduced to gradually add the coupling effect. Newton's method solving for $(\lambda^{(j)}, \boldsymbol{\phi}_r^{(j)})$ is used to trace the evolution of the rigid-body degrees-of-freedom starting from zero frequency at $\beta = 0$ to the coupled eigenvalue at $\beta = 1$. The corresponding fluid part $\boldsymbol{\phi}_f^{(j)}$ of the eigenvector is calculated for the converged solution $(\lambda^{(j)}, \boldsymbol{\phi}_r^{(j)})$ at $\beta = 1$ by solving

$$\left(A_{ff} - \lambda^{(j)} I\right) \boldsymbol{\phi}_f^{(j)} = -A_{fr} \boldsymbol{\phi}_r^{(j)} \tag{18}$$

The computationally expensive part of Eq. (17) is the repeated evaluation of the interaction term $A_{rf} \left(A_{ff} - \lambda^{(j)} I\right)^{-1} A_{fr}$ depending on the solution $\lambda^{(j)}$. For small-sized problems, this matrix can be computed with direct solvers whereas iterative methods have to be applied for industrial test cases [25]. This can lead to convergence problems since the eigenspectrum of the system can contain up to millions of eigenvalues and the flight dynamics eigenvalue might be within the cloud of aerodynamic modes. A Taylor expansion for $\lambda = \lambda_0 + \lambda_\epsilon$ was proposed in [12, 18] to alleviate this problem and speed-up the tracing.

The adjoint eigenvalue problem, the solution of which is needed for the model reduction, is equivalently formulated as

$$\left\{ \left(A_{rr}^T - \lambda^{(j)} I\right) - \beta \left[A_{rf} \left(A_{ff} - \lambda^{(j)} I \right)^{-1} A_{fr} \right]^T \right\} \bar{\boldsymbol{\psi}}_r^{(j)} = 0 \tag{19}$$

while the fluid part of the left eigenvector is then calculated by solving the adjoint problem corresponding to Eq. (18).

The derivation so far has previously been described as Schur complement method. The full order CFD solver is rearranged and directly employed during the solution of the small non-linear eigenvalue problem in Eqs. (17) and (19). The relation to more classical analysis via dynamic derivatives is apparent. This is described next in order to show the equivalence of the interaction term with dynamic derivatives. Substituting the definition of A_{rf} into Eq. (17), the interaction term is expressed as

$$A_{rf} \left(A_{ff} - \lambda^{(j)} I \right)^{-1} A_{fr} = C \frac{\partial \boldsymbol{f}_a}{\partial \boldsymbol{w}_f} \left(A_{ff} - \lambda^{(j)} I \right)^{-1} A_{fr} \tag{20}$$

The term $\left(A_{ff} - \lambda^{(j)} I \right)^{-1} A_{fr}$ is associated in Eq. (9) with the response of the fluid unknowns to excitations in the flight dynamics degrees-of-freedom,

$$C \frac{\partial \boldsymbol{f}_a}{\partial \boldsymbol{w}_f} \left(A_{ff} - \lambda^{(j)} I \right)^{-1} A_{fr} = C \frac{\partial \boldsymbol{f}_a}{\partial \boldsymbol{w}_f} \frac{\partial \boldsymbol{w}_f}{\partial \boldsymbol{w}_r} = C \frac{\partial \boldsymbol{f}_a}{\partial \boldsymbol{w}_r} = CQ \tag{21}$$

Thus, the matrix Q describes the transfer function relating flight dynamics motions to the aerodynamic forces by means of complex-valued dynamic derivatives of the aerodynamic system [26, 27]. The direct and adjoint eigenvalue problems in Eqs. (17) and (19) are then rewritten using dynamic derivatives as

$$\left[\left(A_{rr} - \lambda^{(j)} I \right) + \beta CQ \right] \boldsymbol{\phi}_r^{(j)} = 0 \qquad \left[\left(A_{rr}^T - \lambda^{(j)} I \right) + \beta Q^T C^T \right] \bar{\boldsymbol{\psi}}_r^{(j)} = 0 \tag{22}$$

The dynamic derivatives are pre-computed for a finite number of harmonic motions with values of damping and frequency corresponding to real and imaginary pairs in the complex plane. Interpolation techniques are used to calculate values for points not sampled. The latter equations are identical to Eqs. (17) and (19), if Q is computed for each point in the complex plane.

A simplification arises by neglecting the damping during the computation of the aerodynamic influence, similar to the p-k method [28]. As a consequence, the matrix Q would depend on frequency only and pre-computed for simple harmonic motions.

2.3. Data-based modal identification

The snapshot method [23] is adopted to interpolate the response of the coupled CFD-FD system subject to sinusoidal disturbances. A snapshot matrix S of dimension $n \times m$ is obtained by combining m solutions of Eq. (8) for frequencies in the range of interest. The

number of snapshots determines the number of possible modes. Producing the snapshots is the computationally expensive part of the method since m complex-valued linear systems with leading dimension n need to be solved. Equation (8) involves the coupled Jacobian matrix and it can be solved with the same strategies used for the interaction matrix described above, i.e. direct or iterative methods according to the size of the system. POD is then applied to the snapshot matrix S with POD modes $\boldsymbol{\phi}^{(j)}$ defined as

$$\boldsymbol{\phi}^{(j)} = S\boldsymbol{v}_j \qquad \forall j \in [1, m] \tag{23}$$

where each entry of the vector $\boldsymbol{v}_j$ represents the contribution of the corresponding snapshot to the mode $\boldsymbol{\phi}^{(j)}$. The condition that $\boldsymbol{v}_j$ lie along the principal axes of the space spanned by S leads to the eigenproblem

$$\langle S, S\rangle \boldsymbol{v}_j = \sigma_j \boldsymbol{v}_j \qquad \forall j \in [1, m] \tag{24}$$

with larger eigenvalues σ_j corresponding to the dominant modes in terms of energy. The negligible computational cost of the reduced model can be further decreased by selecting only a subset of modes [29]. However, this further reduction is not performed in this paper to avoid the arbitrariness of selection criteria.

Contrary to the Petrov-Galerkin projection used for the operator-based approach, the Galerkin one is used for the data-based ROMs instead. As a result, both the modal bases Φ and Ψ contain the same POD modes and they satisfy Eq. (11). The method presented here does not depend on the nature of the disturbance $\boldsymbol{u}_d$. However, the POD technique will be applied in the following to gust encounter simulations.

2.4. Coupled flight dynamics and aerodynamics model

The CFD code uses a meshless scheme to solve the Euler, laminar and Reynolds-averaged Navier–Stokes equations (with the Spalart–Allmaras turbulence model) [30, 31]. The unknowns are stored at each point and the spatial discretisation is performed on a stencil of neighbouring points. Osher's approximate Riemann solver is used to evaluate the convective fluxes between each point and the points in its stencil. The gradients of the flow variables are reconstructed with the least squares method and used to provide a higher order reconstruction of the interface values for the Riemann problem. A fully implicit scheme is applied using local time stepping for convergence acceleration, while the unsteady, time-dependent equations are solved with a dual-time integration scheme. Mesh deformation is available in the CFD solver and performed with radial basis function interpolation [32]. The iterative solver used for linear systems resulting from both the fully-implicit scheme and to perform LFD computations is the generalised minimal residual solver (GMRES) with complex arithmetic [33]. Preconditioning uses incomplete lower-upper factorisation.

Gusts are implemented in the full order model with disturbance velocity approach [34]. The so-called gust matrix $\frac{\partial \boldsymbol{R}}{\partial \boldsymbol{u}_d}$ can be calculated by finite differences and it contains changes in the residual due to mesh velocity. The vector $\hat{\boldsymbol{u}}_d$ depends on the gust shape to be simulated since it represents the phase lag between points due to the excitation. The flight

dynamics residual does not directly depend on the gust disturbance and $\frac{\partial \boldsymbol{R}}{\partial \boldsymbol{u}_d}$ is padded with zeros accordingly.

The coupling between rigid-body dynamics and aerodynamics is performed with a modular approach resulting in a strongly coupled system. At each inner iteration, the position and velocity of grid points are modified according to the motions (translation and rotation) provided by the flight dynamics module. For longitudinal problems, the flight dynamics state vector $\boldsymbol{w}_r$ contains 6 unknowns, specifically $\boldsymbol{w}_r = [u, v, q, x, z, \theta]^T$. The horizontal and vertical translations, x and z, are referred to inertial axes [22]. The rigid rotation θ is the Euler angle describing the orientation of the body relative to the inertial reference frame while q is the related angular velocity. The horizontal and vertical velocities in the body reference frame u and v are assumed variations from the corresponding velocities U_e and W_e at equilibrium condition. These are defined as $U_e = U_\infty \cos\alpha_0$ and $W_e = U_\infty \sin\alpha_0$ with U_∞ and α_0 denoting velocity and angle-of-incidence in steady flight. The flight dynamics state vector is updated by integrating the equations of motion [21],

$$\begin{aligned} \frac{\mathrm{d}u}{\mathrm{d}t} + W_e q &= \frac{F_x}{m} & \frac{\mathrm{d}x}{\mathrm{d}t} &= (U_e + u)\cos\theta + (W_e + w)\sin\theta \\ \frac{\mathrm{d}v}{\mathrm{d}t} - U_e q &= \frac{F_z}{m} & \frac{\mathrm{d}z}{\mathrm{d}t} &= -(U_e + u)\sin\theta + (W_e + w)\cos\theta \\ \frac{\mathrm{d}q}{\mathrm{d}t} &= \frac{M_y}{I_\theta} & \frac{\mathrm{d}\theta}{\mathrm{d}t} &= q \end{aligned} \tag{25}$$

with mass m and moment of inertia I_θ in the longitudinal plane. The terms F_x, F_z and M_y represent the horizontal force, vertical force and pitching moment accounting for aerodynamic forces from the CFD solver as well as body forces such as gravity. The properties of the system are expressed by two non-dimensional quantities, specifically the radius of gyration $r_\theta = \sqrt{I_\theta/(mb^2)}$ and mass ratio $\mu = m/(\pi\rho b^2)$, where ρ is the fluid density. This is achieved by defining a reference length b, which corresponds to half a wing chord length in this work, a non-dimensional time $\tau = tU_\infty/b$ and reformulating Eq. (25) accordingly.

3. Results

Results are presented for two transonic-flow aerofoil test cases. The first is a NACA 0012 aerofoil solving the Euler equations and focusing on the detailed description of the operator-based identification technique. In addition, a comparison with the data-based method is provided. The tools are then applied to a more complex wing-tail configuration solving the RANS equations. A LFD solver is used throughout, except for reference solutions which use the non-linear time-accurate solver. The LFD formulation in the in-house CFD code has previously been verified in [29, 35].

3.1. NACA 0012 single aerofoil

The computational domain is discretised with 7860 points. The small size of the model allows for a detailed investigation to identify potential problems arising during the identi-

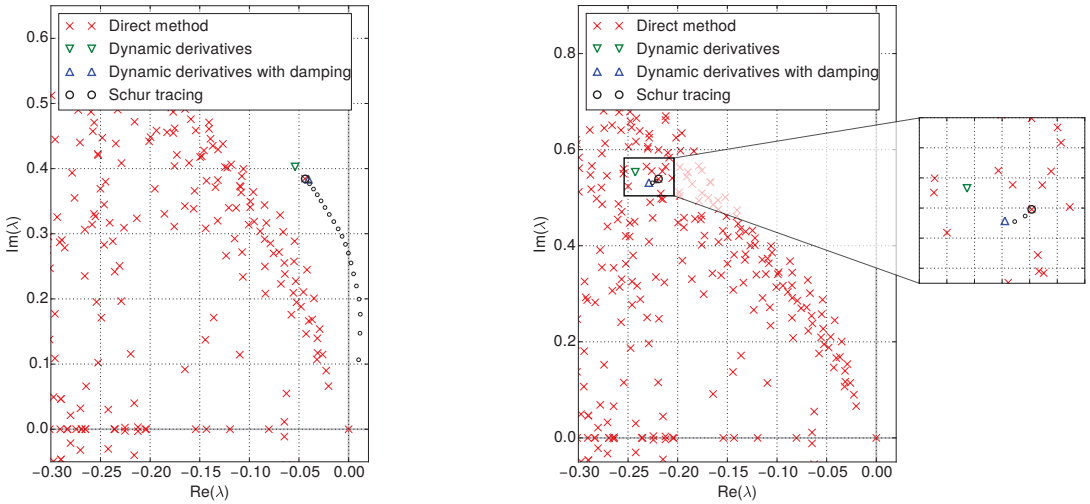

(a) Identification at $\mu = 100$

(b) Identification at $\mu = 35$

Figure 1: Eigenspectrum for operator-based identification.

fication procedure and discuss remedies. The steady state is calculated at a Mach number of 0.75 and 0 deg angle-of-attack. The radius of gyration is $r_\theta = 0.5$ and two mass ratios are investigated, as discussed below. The drag is assumed to be constantly balanced by a thrust so that the rate of horizontal speed $\frac{\mathrm{d}u}{\mathrm{d}t}$ is zero. Without affecting the generality of the approach, the centre of mass is located at the leading edge to have a stable flight dynamics model for many flow conditions.

Regarding the operator-based identification, two flight dynamics modes related to vertical translation and rotation are expected to play a key role [21] since the focus is on the short-term longitudinal motions. The mode corresponding to the horizontal degree-of-freedom does not contribute to the short-term response of the system and is omitted [22]. It was found that the eigenvalue corresponding to the vertical translation mode remains close to the origin and is thus easy to calculate. The short period mode originating from the rigid rotation on the other hand is more challenging to identify and details are discussed in this section. The eigenvalue associated to the short period moves from the origin of the complex plane for in-vacuum conditions, to a new, as yet undefined, position when aerodynamics is imposed.

The two values of mass ratio, $\mu = 100$ and $\mu = 35$, lead to distinct system behaviours. Identification results are shown with parts of the complete eigenspectrum in Fig. 1. Note that only the size of the full order problem allows a direct calculation of the eigenvalues of the coupled Jacobian matrix and this is not the case in general. A number of 250 eigenvalues close to a shift of $0.3i$ were thus extracted using MATLAB®, specifically direct methods implemented in the function `eigs`.

Regarding the case with mass ratio of 100, presented in Fig. 1(a), the eigenvalue corresponding to the short period mode, traced using the Schur complement method, is outside the cloud of fluid eigenvalues. The tracing is shown with the parameter β increasing from

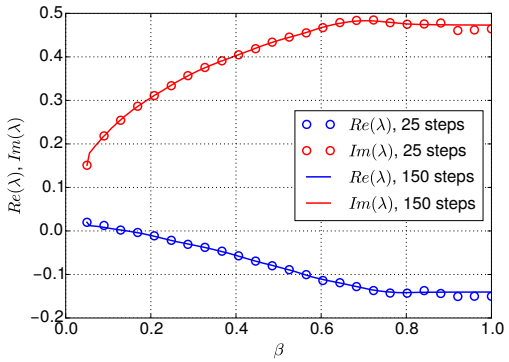

(a) Real and imaginary part of eigenvalue

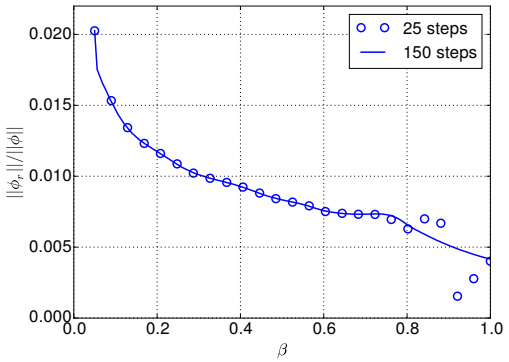

(b) Norm of flight dynamics part of eigenvector compared to norm of whole eigenvector

Figure 2: Evolution of traced eigenpair as function of parameter β for an unsuccessful tracing.

zero to one in 20 steps. For each step Newton's method was used to calculate the eigenpair for the new value of β using the previous converged solution as initial guess. At $\beta = 0$, when all the eigenvalues related to the flight dynamics degrees-of-freedom are located in the origin of the eigenspectrum, the selection of the mode to trace is based on a different rigid-body eigenvector of A_{rr} as initial guess. The Schur complement method provides an exact solution to the eigenvalue problem, as can be seen by comparison with the direct method. In addition, the figure includes the results based on the approximation of the interaction matrix with dynamic derivatives. The matrix Q was pre-computed at 7 reduced frequencies linearly distributed in the interval ranging from 0 to 0.8. Linear interpolation is used to evaluate Q for intermediate reduced frequencies. Adding more samples does not change the final results. The approximation of discarding the damping when calculating the interaction term Q leads to slightly different results compared to the Schur complement method. However, the error introduced should be seen in relation to the computational cost which is much lower for the dynamic derivatives method. A trade-off between the two approaches is the inclusion of damping for the calculation of the dynamic derivatives. The pre-computation of Q was extended to non-harmonic motions corresponding to a finite number of points in the complex plane. The set of 7 samples already available at zero damping was extended calculating the dynamic derivatives at the same frequencies but with a damping corresponding to the solution provided by the basic dynamic derivatives method. Note that this does not represent an optimised strategy which should focus on a refined local sampling instead. Two-dimensional linear interpolation was then used for points in the complex plane. The assumption of a linear behaviour with respect to the damping improves the final solution which is now closer to the exact result provided by the Schur complement method.

The case for the lower mass ratio of 35, when the eigenvalue related to the short period resides inside the cloud as shown in Fig. 1(b), is significantly more challenging. The presence of fluid eigenvalues around the target eigenvalue misleads the Schur tracer converging to fluid eigenpairs during the tracing procedure instead. This is particularly critical when

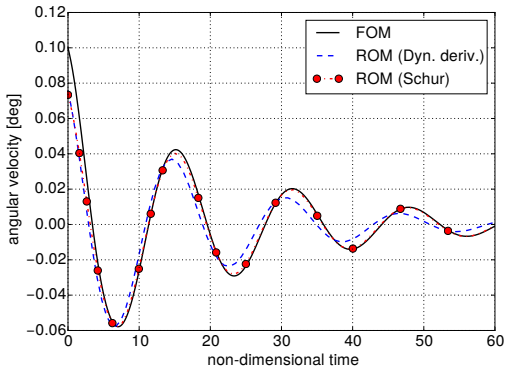

(a) Angular velocity at $\mu = 100$

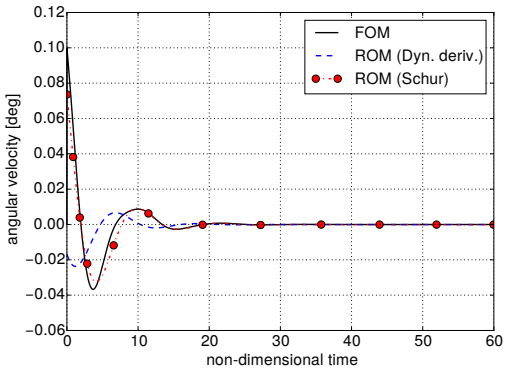

(b) Angular velocity at $\mu = 35$

Figure 3: Response to initial disturbance in angular velocity of $q = 0.1\,\mathrm{deg}$.

iterative methods are used to evaluate the interaction matrix, since the iterative solver might not converge at all. The eigenvalue evolution during an unsuccessful tracing is shown in Fig. 2(a). In addition, the relative importance of the flight dynamics part of the eigenvector $\boldsymbol{\phi}_r$ compared to the whole eigenvector $\boldsymbol{\phi}$ is depicted in Fig. 2(b). When $\beta \approx 0.8$ the Schur tracer starts iterating around an eigenpair for which the eigenvalue is not changing any more. However, it is clear from Fig. 2(b) that the ratio $^{||\boldsymbol{\phi}_r||}/_{||\boldsymbol{\phi}||}$ decreases at every iteration for $\beta > 0.8$ while λ is nearly constant. The Schur tracer is converging to an eigenvector whose flight dynamics part is becoming less important. A way to alleviate this problem, while adding to the computational cost, is to increase the number of steps for the tracing. However also this strategy fails for this case since increasing the number of steps from 25 to 150 does not improve the results. The problem is overcome using the dynamic derivatives method to calculate a first approximation of the solution. This method is not sensitive to the presence of fluid eigenvalues since it uses sample points to reconstruct Q. The resulting eigenvalue and eigenvector were used as initial solution for the Schur complement method which was able to converge to the exact solution in few iterations.

The same techniques for the identification of the short period were applied to the vertical translation mode. The solutions to the corresponding adjoint problems in Eqs. (19) and (22) provided the adjoint eigenpairs required for the model reduction. Identifying these eigensolutions is trivial once the direct solution is known. Two ROMs were built using the modes provided by the Schur complement method and the dynamic derivatives approach. Results using dynamic derivatives calculated for damped harmonic motions are not included for sake of brevity since they do not differ significantly from the ones produced with the Schur complement method.

Initial disturbance analyses with angular velocity $q(t = 0) = 0.1\,\mathrm{deg}$ per non-dimensional time-unit were performed for both mass ratios and presented in Fig. 3. For $\mu = 100$ results from the reduced model based on the Schur complement method matches the reference full order model obtained with Eq. 4. Small differences are visible in the first two peak values presumably due to the broadband excitation given by the initial disturbance analysis. This

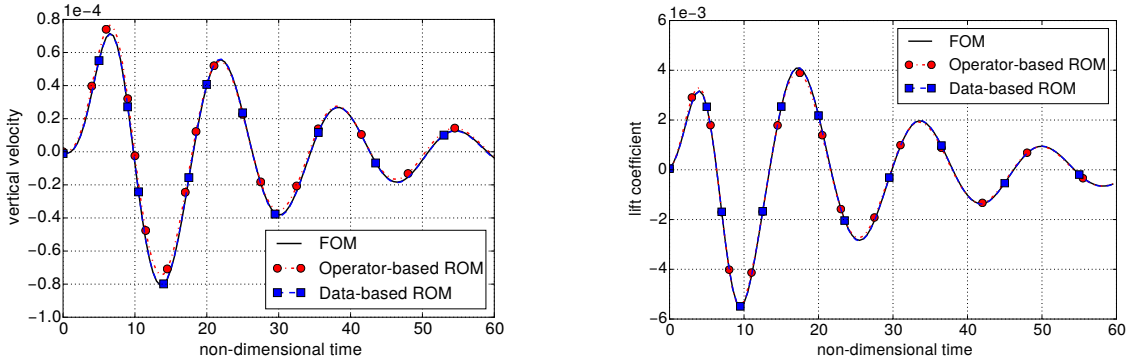

(a) Vertical velocity

(b) Lift coefficient

Figure 4: Response to gust encounter for a '1-cos' gust of amplitude $V_g = 0.1\%$ free-stream velocity and gust wavelength of 10 chord lengths at $\mu = 100$.

can excite flight dynamics as well as quickly-decaying aerodynamic modes, leaving the system response to the dominant modes. Results from the dynamic derivatives method show an underestimation of peak values and a general frequency shift due to the approximation made. The case for $\mu = 35$ presented in Fig. 3(b) provides a stronger damped response as expected from the real part of the short period eigenvalue. The reduced model built with the dynamic derivatives method is less accurate for the transient decay even though the transition to the new equilibrium state, characterized by a return to zero velocity, is captured. In the following, the discussion focuses on the Schur complement method only.

The reduced model was extended for external disturbances to analyse flight dynamics effects during gust encounter. Results at $\mu = 100$, when flight dynamics is more relevant to the system, are given in Fig. 4, depicting flight dynamics response and lift coefficient for the encounter with a travelling '1-cos' gust with intensity $V_g = 0.1\%$ of free-stream velocity and wavelength $L_g = 10$ chord lengths. Only vertical velocity is shown since similar agreement is obtained for all the flight dynamics degrees-of-freedom. Results from the operator-based Schur complement method show a good agreement with the full order model. Some differences arising in the peak values might depend on the choice of modes lacking information to completely describe the aerodynamic phenomena. This problem will be analysed in detail below. The application of the data-based method requires the '1-cos' time-domain gust signal to be translated in the frequency domain as sum of sinusoidal gusts at distinct frequencies. Specifically, snapshots were calculated for 25 reduced frequencies linearly distributed in the range 0 to 2. A convergence analysis was performed to ensure that the minimum number of snapshots was adopted and results did not change when including additional snapshots. Thus, results in Fig. 4 were produced with 25 POD modes. Using the data-based ROM, loads and motions are evaluated accurately for both transient decay and final steady state. The case with $\mu = 35$ is not discussed at this point since a case leading to similar results is presented in the next section.

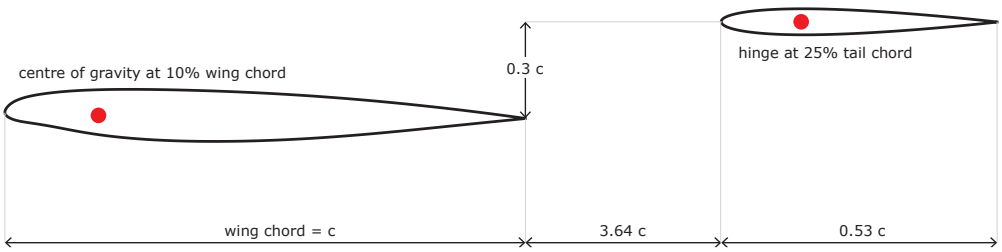

Figure 5: Wing-tail configuration analysed for longitudinal dynamics.

3.2. Wing-tail configuration

An application of the methods to a more complex configuration, representative of the longitudinal dynamics of a large civil aircraft, is presented. The model is composed of a supercritical Crank aerofoil for the main wing and a NACA 0008 for the tail as shown in Fig. 5. The centre of gravity, which is also the rotation point for moment calculation, is at 10% of the wing chord, and the tail hinge axis is at 25% of its chord. The RANS equations are discretised on 115,224 grid points with the far-field 100 chord lengths away. The fluid flow is transonic at Mach number of 0.75 and Reynolds number based on the chord length of the main wing of 7 million. The radius of gyration is $r_\alpha = 3.5$, while two values for the non-dimensional mass ratio μ are investigated, specifically $\mu = 730$ and $\mu = 73$. The former corresponds to a condition for which the flight dynamics modes are outside the cloud of the eigenvalues and they are dominant modes for the system. A physical interpretation is a combination of mass and moment of inertia for which the short period mode has low damping and the related eigenvalue is close to the imaginary axis of the complex plane. The mass ratio of $\mu = 73$ on the other hand corresponds to a large civil aircraft flying at 10 km altitude.

The initial equilibrium condition, independent of mass ratio, is obtained with an iterative trimming procedure based on the Broyden method [36]. Target values of lift and moment coefficients, $C_L = 0.15$ and $C_M = 0$, are chosen based on representative level flight conditions. At each trimming iteration, tail rotation is imposed with mesh deformation and loads are calculated with few iterations of a steady-state computation. Thrust balances the drag at equilibrium condition. The converged angle of attack and tail rotation are 0.91 and -0.85 deg, respectively, with clockwise positive rotations. The resulting steady flow field, used as reference point for the subsequent linearisation, is shown in Fig. 6.

The operator-based identification was first applied. Similar to above, the dynamic derivatives method was used to provide the Schur complement tracer with an initial guess. The derivatives were calculated at 10 reduced frequencies in the range 0 to 0.5. The same frequencies were sampled at 3 different damping values in the range -0.1 to 0. Figure 7 presents results of the mode identification for both mass cases. Direct methods were used to calculate some eigenvalues of the coupled Jacobian matrix which are shown as a reference solution. These reference eigenvalues were obtained using multiple shifts distributed along the positive part of the imaginary axis. The short period mode was identified. The phugoid mode, which differs significantly in terms of frequency from the short period, was identified as well

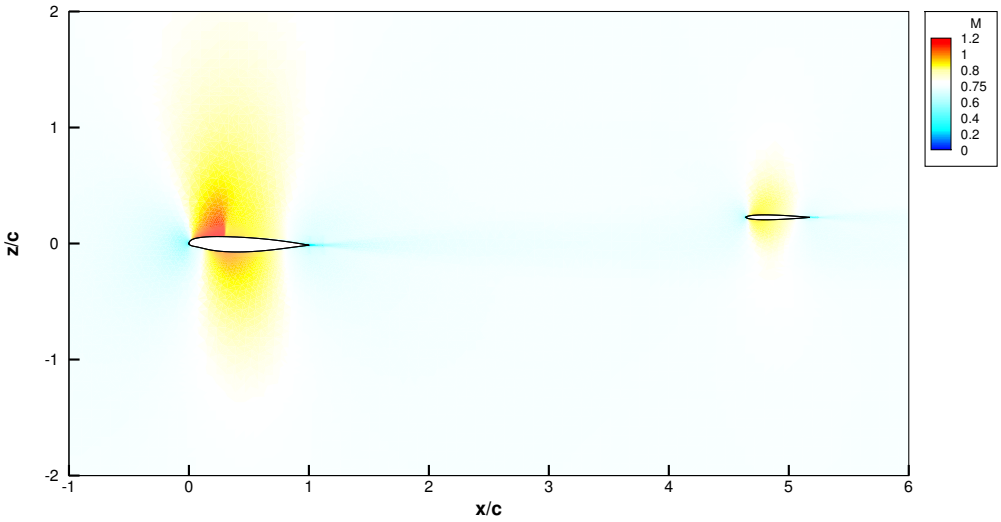

Figure 6: Mach number field resulting from trimming procedure.

by retraining the horizontal degree-of-freedom. No noticeable difference was found between the three identification methods for $\mu = 730$. Assuming the dynamic derivatives are function of frequency only is an acceptable approximation since the target eigenvalues are very close to the imaginary axis. In contrast, Fig. 7(b) depicts a short period inside the cloud of eigenvalues for $\mu = 73$. Both values of phugoid and short period are affected by an error when obtained with dynamic derivatives. These are calculated discarding the real part of the eigenvalue in Eq. (22) and this leads to underestimation of frequency and damping for the short period as well as overestimation of the phugoid frequency. Including the damping improves the results and provided an initial guess for the Schur complement method. The refinement with the Schur tracing led to the same results obtained by the direct method.

Once direct and adjoint eigenpairs are identified, the model reduction is applied and the number of degrees-of-freedom is reduced from 576,126 to 2. Results for an initial disturbance in the angular velocity are shown for $\mu = 730$ in Fig. 8(a). As expected for this case, full and reduced models produce the same results. Regarding the gust encounter presented in Fig. 8(b), no appreciable difference is visible between the ROMs since they provide similar results. The disturbance is a '1-cos' gust with an amplitude of 0.1% of the free-stream velocity and a gust wavelength of 20 wing chord lengths. The system response is well reproduced by all the operator-based approaches. The modes from the coupled Jacobian matrix provide a good basis for the model reduction of a complex geometry when the flight dynamics modes are dominant. A small difference between full order model and ROMs is shown in the first part of the simulation, up to the first peak value, since no information is contained in the modes to represent the external disturbance. Overall, the ROMs match the full order results of initial disturbance and gust encounter simulations and therefore the focus will be on the more challenging mass case $\mu = 73$ from now on.

For this case, an initial disturbance in the angular velocity of $q(t = 0) = 0.1\,\mathrm{deg}$ (per non-dimensional time-unit) leads to the response shown in Fig. 9(a). The mode identifica-

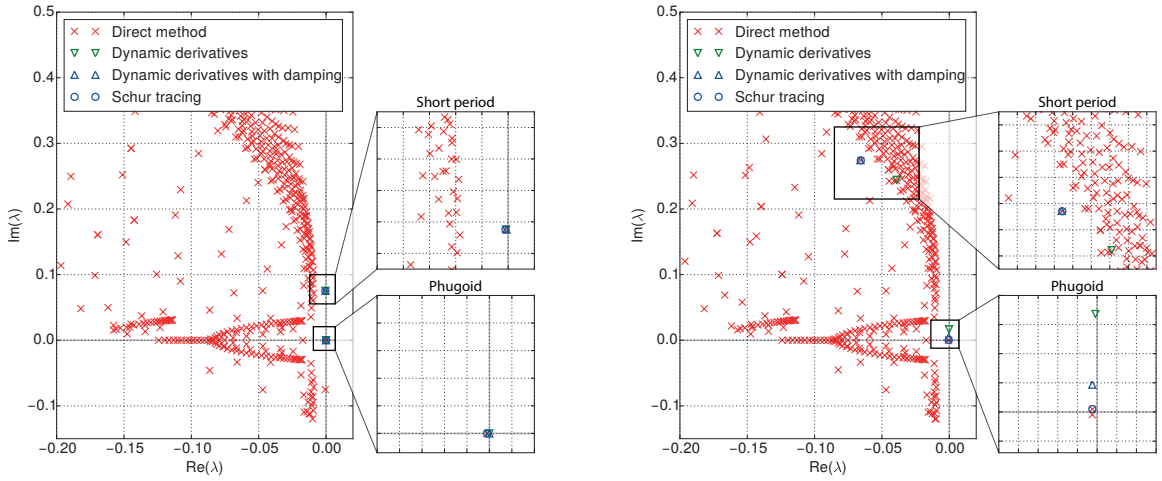

(a) Identification at $\mu = 730$

(b) Identification at $\mu = 73$

Figure 7: Results of operator-based mode identification compared to reference solution.

tion performed while discarding the real part of the eigenvalue for the interaction matrix is not effective when the flight dynamics eigenvalues are strongly coupled (or interacting) with aerodynamics. Using the dynamic derivatives leads therefore to lower accuracy. Including the damping produces results which are very close to the ones from the exact Schur complement method. Hence, for sake of clarity only the latter will be kept in the following as reference for the operator-based identification. The comparison between full order model and ROM based on Schur tracing shows that the reduced model is able to reproduce the general trend of the system response. Initial conditions have a small offset and results match the reference when oscillations decay. A phase lag and an underestimation of the peak values is visible however during the transient. An explanation to consider is that the two modes included in the modal basis contain only part of the required information.

This assumption is investigated further by calculating eigenpairs with the direct method and including them in the modal basis. Although this cannot be used as a model reduction technique because of the prohibitive computational power required to extract eigensolutions, it does provide a posteriori confirmation. Results of the model reduction including an increasing number of modes surrounding the short period and phugoid is depicted in Fig. 9(b). Results for the model reduction performed with the operator-based identification are included as reference. Besides the two flight dynamics modes, 48 and 128 additional eigenpairs closest to the short period are subsequently added to the modal basis. Results for the transient improve gradually and with 130 modes the system response is well represented. Another set of 80 eigenpairs closest to the phugoid is then added to the modal basis, for a total of 210 modes. This further improves the results for peak values. Information about rigid body motions is distributed in the eigenpairs surrounding the flight dynamics eigenpairs highlighting the strong coupling. Hence, the two flight dynamics modes contain only part of the information required for the model reduction. In those cases, modes from the

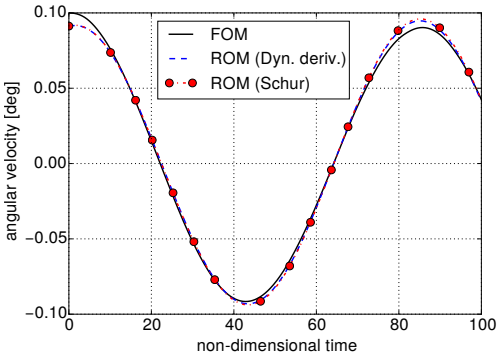

(a) Response to initial disturbance in angular velocity of $q = 0.1\,\text{deg}$

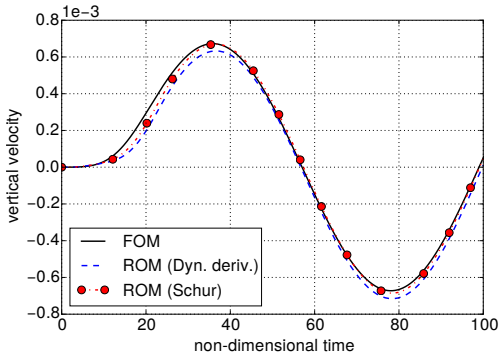

(b) Response to a '1-cos' gust with intensity $V_g = 0.1\%$ of the free-stream velocity and wavelength of 20 wing chords

Figure 8: Results for initial disturbance and gust encounter simulations for mass case $\mu = 730$.

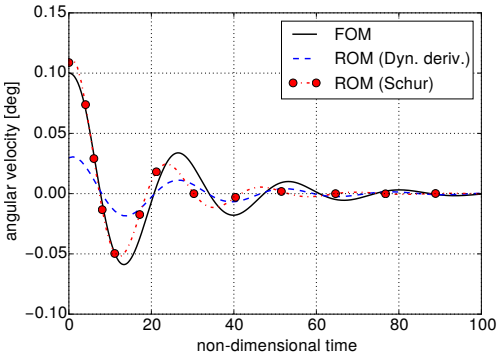

(a) ROMs built using modes from operator-based identification

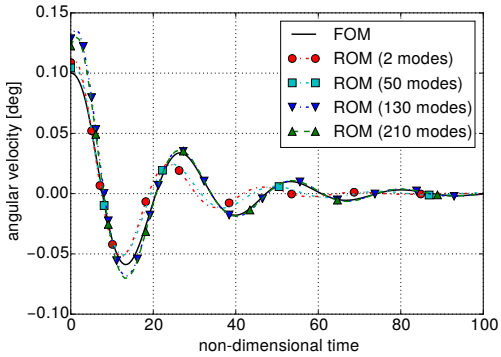

(b) Effect of including eigenpairs surrounding short period and phugoid

Figure 9: Response to initial disturbance in angular velocity of $q = 0.1\,\text{deg}$ at $\mu = 73$.

operator-based identification might not be sufficient to reproduce accurately the full order results.

The analysis is now expanded toward external disturbances. Results are presented in Fig. 10 for a '1-cos' gust with intensity $V_g = 0.1\%$ of free-stream velocity and gust wavelength $L_g = 10$ chord lengths. A preliminary comparison is made between reference results from CFD-only and coupled gust simulations. No motion is allowed for CFD-only simulations and Fig. 10(b) shows the lift build-up followed by a smooth decay. In contrast, results of the coupled approach produce oscillations. Regarding lift coefficient, the amplitude of the first oscillation is lower in comparison to CFD-only simulations because part of the energy goes into the rigid body motions. The subsequent system response is composed of few decaying oscillations. The same simulation was performed with an operator-based ROM containing the short period and phugoid modes. Concerning the vertical velocity in Fig. 10(a), results converge to the initial equilibrium, whereas the transient is not reproduced well, which is

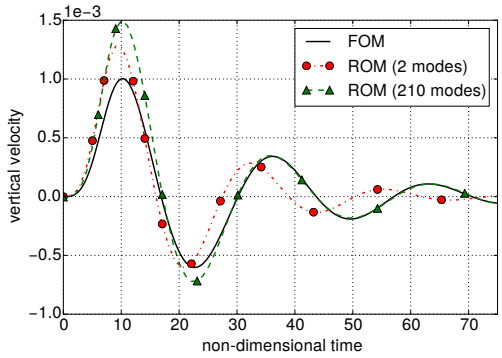

(a) Vertical velocity

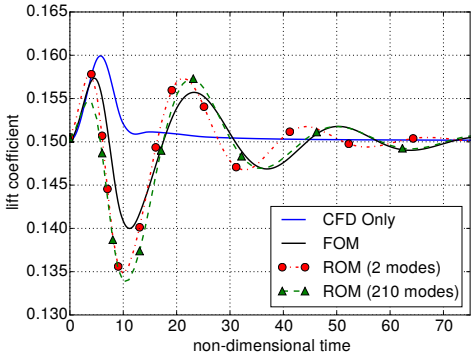

(b) Lift coefficient

Figure 10: Response to gust encounter for a '1-cos' gust of amplitude $V_g = 0.1\%$ free-stream velocity and gust wavelength of 10 chord lengths at $\mu = 73$.

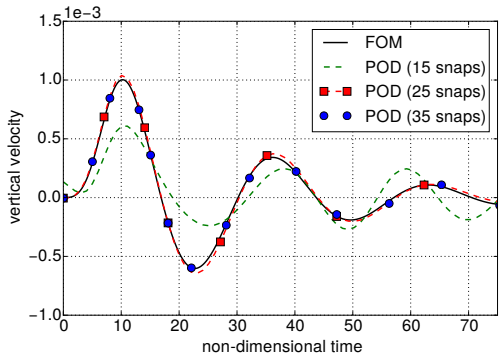

(a) Vertical velocity

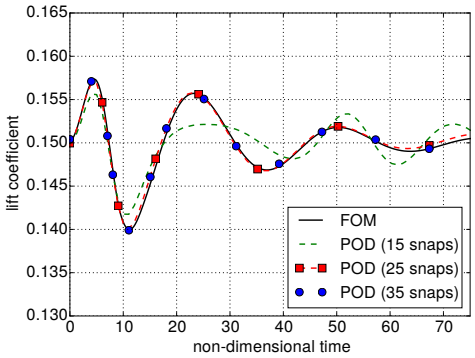

(b) Lift coefficient

Figure 11: Response to gust encounter for a '1-cos' gust of amplitude $V_g = 0.1\%$ free-stream velocity and gust wavelength of 10 chord lengths at $\mu = 73$.

highlighted by phase lag and underestimation of peak values. The first peak is due to the aerodynamic disturbance and it is not fully captured by the flight dynamics modes. This observation is supported in Fig. 10(b) for lift coefficient, where the amplitudes of the first few oscillations are not properly described either. The strategy of adding the 208 modes surrounding the short period and phugoid to the modal basis improves the results. However, differences are still visible in the first two oscillations of vertical velocity. Subsequent fluctuations are fully captured by this reduced model as well as the asymptotic value for the final equilibrium. The same trend is visible for lift coefficient and the initial build-up is not completely reproduced. These modes, all coming from the coupled Jacobian matrix, are not able to fully reproduce the effects of a pure aerodynamic external disturbance. The first peak values depending mostly on the external disturbance are therefore not accurately captured.

A strategy to overcome this problem is to use the data-based approach to calculate

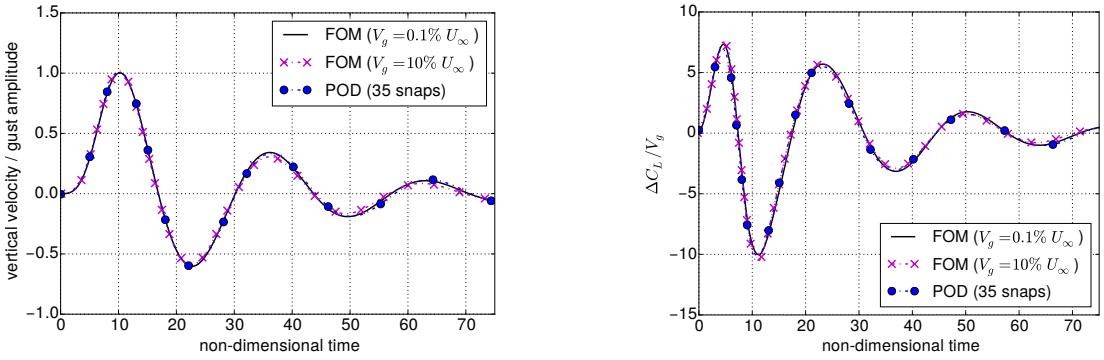

(a) Vertical velocity

(b) Lift coefficient variation

Figure 12: Response to gust encounter for '1-cos' gusts with amplitudes of $V_g = 0.1\%$ and $V_g = 10\%$ free-stream velocity and gust wavelength of 10 chord lengths at $\mu = 73$.

modes for the model reduction. The modal basis containing POD modes was computed with a number of snapshots ranging from 15 to 35. Snapshots were distributed linearly in the frequency range between 0 and 2 to investigate a typical range of gust lengths and optimisation of the sampling process is not attempted. The quality of results depends on the number of snapshots used as shown in Fig. 11. Model reduction performed with 15 POD modes led to results not matching the full order model since a different decay ratio and a phase lag are clearly identified for the vertical velocity. The values for lift are underestimated at the beginning and the subsequent oscillations are not reproduced properly. Increasing the number of snapshots provides better results and the full order results are matched with 25 POD modes. Such reduced model is capable of describing accurately the flight dynamics response and aerodynamic forces. Some differences arise for peak values of the vertical velocity after the first few oscillations. Although these differences are negligible, they can be eliminated by further increasing the number of snapshots up to 35. No appreciable difference is visible between the ROM with 35 POD modes and the full order model.

Although the reduced model should be compared to the full order model acting linearly, non-linear effects are investigated by performing a '1-cos' gust simulation with 10 chords wavelength and a large amplitude of $V_g = 10\%$ free-stream velocity. This corresponds to an amplitude similar to EASA regulations [1]. Results are scaled by the gust amplitude and presented in Fig. 12 alongside the linear full order solution and the ROM curve already shown in previous plots and corresponding to an amplitude of $V_g = 0.1\%$ free-stream velocity. For this particular case, a largest difference of $\pm 5\%$ was found between linear and non-linear results, since non-linear effects are weak and they involve mainly peak values.

Based on the results presented, the application of the proposed method is summarised as follow. First, the operator-based identification is performed using dynamic derivatives calculated for 10 reduced frequencies between 0 and 0.5. Secondly, if flight dynamics eigenvalues are far from the imaginary axis, a refinement using the Schur complement method is required. Thirdly, if the focus is on system response to external disturbance, the data-based identification using 25 samples between 0 and 2 provides accurate results.

The computational cost of the ROM can be split in two main contributions. The first involves building the modal bases using LFD calculations for both operator-based and data-based approaches. Obtaining an LFD solution for the wing-tail configuration takes around 7 min on an Intel Xeon E3-1245 CPU (single-core) converging 8 orders of magnitude. The total CPU time is summed as 2 h for operator-based ROM with dynamic derivatives, 7 h for the one with Schur tracing refinement and 3 h for the data-based ROM with 25 samples. The second contribution is given by the integration of the ROM equations and omitted in this calculation since it is negligible. These numbers are compared to the 5 days required by one non-linear full order reference simulation coupling unsteady RANS aerodynamics and non-linear flight dynamics equations for gust encounters on the same single-core hardware. Considering that multiple gust lengths must be analysed during aircraft design, a reduction factor of 100 can be obtained. A recent three-dimensional application is presented in [37] where the method is expanded towards an industrial test case and comparable cost savings are achieved.

4. Conclusions

The work describes an investigation of a model reduction technique for coupled simulations involving flight dynamics and computational fluid dynamics. Model reduction is achieved by projecting a Taylor-expanded full order coupled non-linear residual function onto a modal basis populated with modes representing the system dynamics. An operator-based modal identification technique is adopted as procedure to obtain flight dynamics modes from the coupled Jacobian matrix. This method is suitable for large test cases since it does not rely on the direct calculation of the system's eigenspectrum. An exact formulation is provided with the Schur complement method and an approximation, using dynamic derivatives, is proposed as trade-off between computational cost and accuracy. Operator-based identification focuses on the system behaviour not subject to any external disturbance, resulting in a versatile model which can be easily exploited for stability analysis and to simulate gust encounter when flight dynamics modes are dominant. Alternatively, a data-based formulation using proper orthogonal decomposition is presented for cases when the global modes from the coupled Jacobian matrix are not sufficient to describe the transient dynamics. Data-based reduced models are trained to reproduce the behaviour of the system subject to external disturbance by sampling the full order model at discrete frequencies. In particular, modes resulting from the data-based identification can accurately reproduce the behaviour of the coupled system during gust encounter.

The methods are explored for a basic NACA 0012 aerofoil and a more complex geometry representing the longitudinal dynamics of a large civil aircraft. The reduced model, based on global modes obtained from the operator-based identification, is capable of describing the system dynamics, both homogeneous and subject to external disturbance, when interaction between modes dominated by flight dynamics and modes dominated by aerodynamics is weak. The operator-based identification shows limitations however in stronger coupled situations. In those cases, the reduced model captures the transition between two equilibrium states but not the transient itself. The missing information about the rigid motions resides

in eigenpairs surrounding the flight dynamics modes, and a global-modes reduced model is enhanced when including these neighbouring modes. Based on the results of the test cases presented in the paper, 25 samples needs to be calculated to improve the prediction capability using the data-based identification.

The work presents an approach to treat flight dynamics problems, in the context of high-fidelity computational aerodynamics, similar to the widely-accepted approach for aeroelastic analysis. Global modes and proper orthogonal decomposition modes can describe the dynamics of systems potentially having many millions of degrees-of-freedom. Projection-based model reduction results in an accurate tool for very rapid computational engineering analysis in the multidisciplinary aircraft loads context.

Acknowledgements

The research leading to these results was co-funded by Innovate UK, the UK's innovation agency, as part of the Enhanced Fidelity Transonic Wing project. The authors would like to thank Reik Thormann for providing the wing-tail grid for CFD computations.

References

[1] EASA, "Certification specifications and acceptable means of compliance for large aeroplanes CS-25 amendment 15," 2007.

[2] Slotnick, J., Khodadoust, A., Alonso, J., Darmofal, D., Gropp, W., Lurie, E., and Mavriplis, D., "CFD vision 2030 study: a path to revolutionary computational aerosciences," Tech. rep., NASA Langley Research Center, NASA/CR-2014-218178, 2013.

[3] Drela, M., "Integrated simulation model for preliminary aerodynamic, structural, and control-law design of aircraft," AIAA 99-1394, 1999.

[4] Shearer, C. M. and Cesnik, C. E. S., "Nonlinear flight dynamics of very flexible aircraft," *Journal of Aircraft*, Vol. 44, No. 5, 2007, pp. 1528–1545.

[5] Cook, R. G. and Palacios, R., "Robust gust alleviation and stabilization of very flexible aircraft," *AIAA Journal*, Vol. 51, No. 2, 2013, pp. 330–340.

[6] Patil, M. and Hodges, D., "Flight dynamics of highly flexible flying wings," *Journal of Aircraft*, Vol. 43, No. 6, 2006, pp. 1790–1798.

[7] Ricciardi, A. P., Patil, M. J., and Canfield, R. A., "Evaluation of quasi-static gust loads certification methods for high-altitude long-endurance aircraft," *Journal of Aircraft*, Vol. 50, No. 2, 2013, pp. 457–468.

[8] Raveh, D. E. and Karpel, M., "Nonlinear design loads for maneuvering elastic aircraft," *Journal of Aircraft*, Vol. 37, No. 2, 2000, pp. 313–318.

[9] Palacios, R. and Cesnik, C. E. S., "Static nonlinear aeroelasticity of flexible slenderwings in compressible flow," AIAA 2005-1945, 2005.

[10] Reimer, L., Ritter, M., Heinrich, R., and Kruger, W., "CFD-based gust load analysis for a free-flying flexible passenger aircraft in comparison to a DLM-based approach," AIAA 2015-2455, 2015.

[11] Thormann, R. and Widhalm, M., "Linear-frequency-domain predictions of dynamic-response data for viscous transonic flows," *AIAA Journal*, Vol. 51, No. 11, 2013, pp. 2540–2557.

[12] Badcock, K., Timme, S., Marques, S., Khodaparast, H., Prandina, M., and Mottershead, J., "Transonic aeroelastic simulation for instability searches and uncertainty analysis," *Progress in Aerospace Sciences*, Vol. 47, No. 5, 2011, pp. 392–423.

[13] Timme, S., Badcock, K. J., and Da Ronch, A., "Linear reduced order modelling for gust response analysis using the DLR-TAU code," IFASD-2013-36A, 2013.

[14] Stroscher, F., Sika, Z., and Petersson, O., "Reduced order model of a blended wing body aircraft configuration," *Progress in Flight Dynamics, GNC and Avionics*, Vol. 6, 2013, pp. 635–650.
[15] Ghoreyshi, M., Jiraseck, A., and Cummings, R., "Reduced order unsteady aerodynamic modeling for stability and control analysis using computational fluid dynamics," *Progress in Aerospace Sciences*, Vol. 71, 2014, pp. 167–217.
[16] Da Ronch, A., Badcock, K. J., Wang, Y., Wynn, A., and Palacios, R. N., "Nonlinear model reduction for flexible aircraft control design," AIAA 2012-4404, 2012.
[17] Da Ronch, A., Tantaroudas, N., Timme, S., and Badcock, K., "Model reduction for linear and nonlinear gust loads analysis," AIAA 2013-1492, 2013.
[18] Timme, S., Marques, S., and Badcock, K. J., "Transonic aeroelastic stability analysis using a kriging-based Schur complement formulation," *AIAA Journal*, Vol. 49, No. 6, 2011, pp. 1202–1213.
[19] Gai, G. and Timme, S., "Nonlinear reduced-order modelling for limit-cycle oscillation analysis," *Nonlinear Dynamics*, Vol. 84, 2016, pp. 991–1009.
[20] Woodgate, M. A. and Badcock, K. J., "Fast prediction of transonic aeroelastic stability and limit cycles," *AIAA Journal*, Vol. 45, No. 6, 2007, pp. 1370–1381.
[21] Wright, J. and Cooper, J., *Introduction to aircraft aeroelasticity and loads*, Wiley, 2007.
[22] Cook, M., *Flight Dynamics Principles*, Elsevier, 2007.
[23] Hall, K., Thomas, J., and Dowell, E., "Proper orthogonal decomposition technique for transonic unsteady aerodynamic flows," *AIAA Journal*, Vol. 38, No. 10, 2000, pp. 1853–1862.
[24] Bekemeyer, P., Thormann, R., and Timme, S., "Rapid gust response simulation of large civil aircraft using computational fluid dynamics," RAeS-AAC-O1, 2016.
[25] Xu, S., Timme, S., and Badcock, K., "Enabling off-design linearised aerodynamics analysis using krylov subspace recycling technique," *Computer and Fluids*, Vol. 140, 2016, pp. 385–396.
[26] Rodden, W. and Giesing, J. P., "Application of oscillatory aerodynamic theory to estimation of dynamic stability derivatives," *Journal of Aircraft*, Vol. 7, No. 3, 1970, pp. 272–275.
[27] Da Ronch, A., Vallespin, D., Ghoreyshi, M., and K.J., B., "Evaluation of dynamic derivatives using computational fluid dynamics," *AIAA Journal*, Vol. 50, No. 2, 2012, pp. 470–484.
[28] Hassig, H., "An approximate true damping solution of the flutter equation by determinant iteration," *Journal of Aircraft*, Vol. 8, No. 11, 1971, pp. 885–889.
[29] Bekemeyer, P. and Timme, S., "Reduced order gust response simulation using computational fluid dynamics," AIAA 2016-1485, 2016.
[30] Kennett, D., Timme, S., Angulo, J., and Badcock, K., "Semi-meshless stencil selection for anisotropic point distributions," *International Journal of Computational Fluid Dynamics*, Vol. 26, No. 9-10, 2012, pp. 463–487.
[31] Kennett, D., Timme, S., Angulo, J., and Badcock, K., "An implicit meshless method for application in computational fluid dynamics," *International Journal for Numerical Methods in Fluids*, Vol. 71, June 2012, pp. 1007–1028.
[32] de Boer, A., van der Schoot M.S., and Bijl, H., "Mesh deformation based on radial basis function interpolation," *Computers and Structures*, Vol. 85, No. 11-14, 2007, pp. 784–795.
[33] Saad, Y. and Schultz, M. H., "GMRES: A generalized minimal residual algorithm for solving non-symmetric linear systems," *SIAM Journal on scientific and statistical computing*, Vol. 7, No. 3, 1986, pp. 856–869.
[34] Heinrich, R. and Reimer, L., "Comparison of different approaches for gust modeling in the CFD code TAU," IFASD-2013-36B, 2013.
[35] Thormann, R., Bekemeyer, P., and Timme, S., "Reduced order modelling of gust analysis using computational fluid dynamics," ECOMASS-5441, 2016.
[36] Broyden, C., "A class of methods for solving nonlinear simultaneous equations," *Mathematics of Computation*, Vol. 19, 1965, pp. 577–593.
[37] Pagliuca, G., Bekemeyer, P., Thormann, R., and Timme, S., "Model reduction for gust load analysis of free-flying aircraft," IFASD-2017-148, 2017.